H. Körner and G. Redeker
Deutsche Forschungs- und Versuchsanstalt
für Luft- und Raumfahrt e.V. (DFVLR)
Institut für Entwurfsaerodynamik
Braunschweig

Abstract

New airfoils may bring a substantial improvement in the aerodynamic efficiency of airborne vehicles. A number of new airfoils based on transonic and laminar concept have been designed and investigated at DFVLR. With theoretical design methods and facilities for experimental verification at hand, airfoils for subsonic transports, sailplanes, propellers, helicopter rotors and combat aircraft have been developed.

1. Introduction

An airfoil with good characteristics forms the basis of a successful wing, propeller or rotor design. Application of new ideas in shaping airfoils, based on better physical understanding of the flow, more exact theoretical design methods and improved experimental techniques lead to new airfoils with substantially improved aerodynamic efficiency.

A nowadays already classical way of designing new airfoils is the exploitation of transonic flow on airfoils. This concept, initiated by Pearcey [1], Nieuwland [2] and Whitcomb [3] is still a fascinating subject. Although new aircraft are already flying with such airfoils, the total advantage of this technology has not yet been achieved.

Another physical concept under detailed investigation is the laminar flow option. Although already realized for sailplanes, the break-through for airplanes flying at higher Reynolds numbers still affords a lot of scientific and engineering effort. Not only totally new flow concepts but also devices for flow interference can generate substantial improvements. Here the avoidance of bubbles and separation in general may be cited.

All these new ideas and techniques only have a small chance for realization if an accurate theoretical prediction of flow phenomena is not possible. In this field the progress of numerical methods in the last decade especially in the computation of transonic flow and in the coupling of inviscid flow calculation and viscous correction now allows the design and prediction of two-dimensional airfoils to a high degree of accuracy. This is valid for the region of attached flow.

On the experimental side also new facilities and more accurate measurement techniques give higher confidence in experimental investigation on airfoils.

Based on these facts, airfoil research has a good chance to succeed in the design of airfoils with improved aerodynamic efficiency. Research work in this area has been conducted at the DFVLR Institute for Design Aerodynamics and a number of typical results of this research work will be presented here. This paper contains the description of

- theoretical and experimental tools used within this framework
- airfoils for subsonic transport aircraft
- airfoils for sailplanes
- airfoils for propellers and helicopter rotors
- airfoils for combat aircraft.

2. Methods for airfoil design and verification

New theoretical methods have produced a major break-through in airfoil design. The methods now available allow the solution of complex design tasks as far as the flow is attached. All methods used (Table 1) consist of a combination of

- inviscid flow methods with
- boundary layer methods.

For incompressible flow the Eppler/Somers method is a very efficient one which is based on a conformal mapping procedure in its design part and on a higher order panel method in its prediction part. The boundary layer code used within this method is that of Walz [5]. A number of options can be specified in this design method such as extent of upper and lower surface pressure plateau at specified α, extent and behaviour of recompression in the rear part, trailing edge angle, etc. This method is especially suited for the design of laminar airfoils and has been used for this task in a large number of cases. An extension of this method to subcritical subsonic flow has been given by Radespiel, who introduces a combination of different compressibility rules.

For compressible supercritical flow, a large variety of methods have been published. The methods used are given in the second part of Table 1. For the prediction of the pressure distribution – the airfoil contour given – two methods are in frequent use: the Bauer/Garabedian/Korn/Jameson method and the Jameson FLO6 method. Both methods are based on the finite difference approximation of the full potential equation in

Authors	Option	Method	Comments
Subsonic			
Eppler/Somers [4]	Design and Prediction	Conformal Mapping Higher Order Panel M.	Incompressible Flow
Eppler/Somers, Extension Radespiel [6]	Design and Prediction	Conformal Mapping Higher Order Panel M.	Subsonic, Subcritical Flow
Transonic			
Bauer/Garabedian/ Korn/Jameson [7]	Prediction	FDM, FPE	Non-conservative
Jameson FLO6 [8]	Prediction	FDM, FPE	Non-conservative or Conservative
Nandanan/Stanewsky/ Inger [9]	Prediction	FLO6	Special Treatment for Shock-Boundary-Layer Interaction
Sobieczky [10]	Design and Prediction	FLO6 + Elliptic Continuation	
McFadden [11]	Design and Prediction	Inverse BGKJ Method	Non-conservative

Table 1 Design and prediction methods for airfoils

a transformed mesh to fulfill the boundary condition in an exact way. The method of Nandanan/Stanewsky and Inger allows a special treatment of the shock-boundary-layer interaction.

Two different design methods are used: the method of elliptic continuation and the inverse BGKJ code. The principle of elliptic continuation at first described by Sobieczky allows the redesign of an existing airfoil with shock to a shockfree design. In this method the redesign is restricted to the contour beneath the supersonic region. This new contour fits with the remaining subsonic contour, but a gap at the rear end of the supersonic contour may occur. This brings the necessity to adjust the trailing edge contour, which leads to an iteration process, solving alternatively the design and analysis problem. As analysis method within this procedure the Jameson FLO6 method is used.

The alternative choice to this design method is the inverse BGKJ method by McFadden. In this method the velocity distribution and the critical velocity have to be specified and the airfoil contour can be evaluated. Although this is mathematically an ill-posed problem, this method works well on condition that only small modifications to existing airfoils are wanted or the existence of a solution is known a priori. This method, too, works in an iteration cycle, beginning with a first guess of the contour. All methods have viscous corrections included. The boundary layer methods used are those of Nash/ McDonald, Walz or Rotta.

Theoretically designed airfoils need an experimental verification in windtunnel or free flight. Both methods have been used for the investigations described here. The experimental tools mainly used within this work are the

- Transonic Windtunnel Braunschweig (TWB) [12],
- Flying Airfoil Testbed on the sailplane "JANUS" [13].

The Transonic Windtunnel Braunschweig (TWB) is a blow-down windtunnel which is especially suited for airfoil investigations at subsonic and transonic flow ($0.4 \leq M \leq 0.95$). The rectangular test section (34 cm x 60 cm) with slotted walls at top and bottom allows to test airfoil models with 15 cm chord length (maximum 20 cm) and 34 cm span (Figure 1). This leads to a

- windtunnel height/airfoil chord of 4.0 (3.0)*
- and a geometric aspect ratio of 2.2 (1.7)*

* The numbers in the brackets are for an airfoil chord of 20 cm.

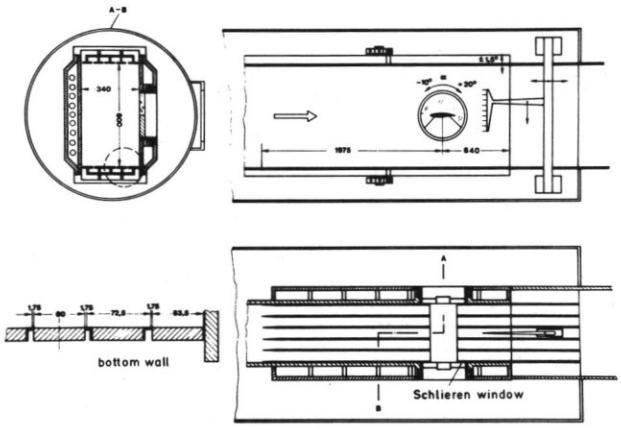

Fig. 1 Transonic Windtunnel Braunschweig (TWB) of DFVLR

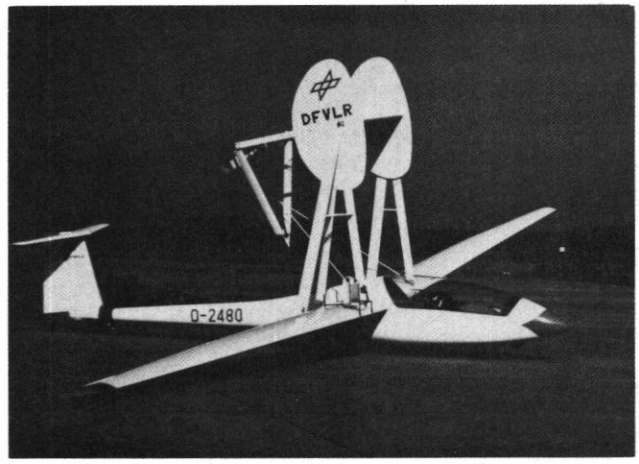

Fig. 2 Flying testbed on the sailplane "JANUS"

which is usual for airfoil investigations. The width of the slots has been optimized to achieve a zero blockage correction. This has led to an open area ratio of $\tau = 2.35\%$. With a maximum pressure in the test section of 4.5 bars a Reynolds number of $Re \approx 10^7$ ($1.4 \cdot 10^7$) can be achieved.

In a routine investigation the subsequent data are provided from the experiment

- static pressure on the airfoil in approximately 50 points on the contour,
- total and static pressure in wake at approximately 360 points.

Lift and pitching moment coefficient are evaluated from the contour pressure, drag coefficient from the wake traverse.

An interesting alternative to windtunnel investigation is the verification of airfoil characteristics in free flight. Due to the difficulties arising here we have concentrated up to now on test with sailplanes. Two directions have been successfully exploited:

- modification of an existing sailplane wing by incorporating a new airfoil on a part of the wing,
- installation of an airfoil testbed on a "JANUS" sailplane.

The modification of an existing wing is a practical procedure although static pressure measurements on the surface cannot be achieved. On the other side a wake traverse allows the determination of the drag and some reference holes on the wing in connection with global values give an indication of the c_L achieved. Furthermore oilflow pictures can be made which give sufficient informations about the flow behaviour.

A more stringent approach is the Flying Airfoil Testbed on the sailplane "JANUS" (Fig. 2). This two-seater sailplane has been equipped with a testbed, which allows the investigation of an airfoil between two endplates. The main geometric data of airplane and test arrangement are given in Table 2. Lift, pitching moment and drag coefficients can be deduced from the static pressure around the airfoil and the wake measurement. In order to get these informations up to 70 pressure holes are drilled into the test wing surface and a rake with 70 probes is installed behind the wing. Investigations with this test arrangement can be done in a speedrange from 80 km/h up to 180 km/h ($0.06 < Ma < 0.13$) and the Reynolds numbers achieved are $0.7 \cdot 10^6 < Re < 4 \cdot 10^6$.

JANUS	
Overall length	8.57 m
Overall span	18.2 m
Wing chord at root	1.2 m
Flying Airfoil Testbed	
Test wing chord length	0.4 ÷ 1.2 m
Span between endplates	2.0 m
Effective aspect ratio	5 ÷ 1.7
Distance of test wing above main wing	2.5 m

Table 2 Main geometric data of the sailplane JANUS with airfoil testbed

Flight tests with this arrangement have been conducted for the development of new sailplane airfoils. Since these airfoils always have laminar option, experiences in this area have a large impact on airfoil development in the other areas. Furthermore it has to be mentioned that this work is done in close co-operation with the "Akademische Fliegergruppe (AKAFLIEG) Braunschweig", a group of aeronautical students at the Technical University Braunschweig.

3. Subsonic transport aircraft

As a subsonic transport aircraft is flying most of its time at an optimum cruise condition airfoils for such type of aircraft are designed for one flight condition, the optimum cruise. Thus the design aims for the airfoil can be summarized as follows:

- shockfree isentropic recompression pressure distribution near the design condition (specified Mach number M and lift coefficient c_L),
- best aerodynamic efficiency $c_L/c_D \cdot M$,
- good off-design characteristics, that means sufficient safety margin Δc_L and ΔM from the buffet onset boundary,
- thickness ratio as high as possible.

Former investigations on types of pressure distributions for transonic airfoils indicated [14] that satisfactory off-design behaviour could be achieved by a slopy roof-top type of pressure distribution. Under these premises the development of transonic airfoils was started at DFVLR in the framework of the Civil Component Programme (ZKP) initiated by the Ministry for Research and Technology.

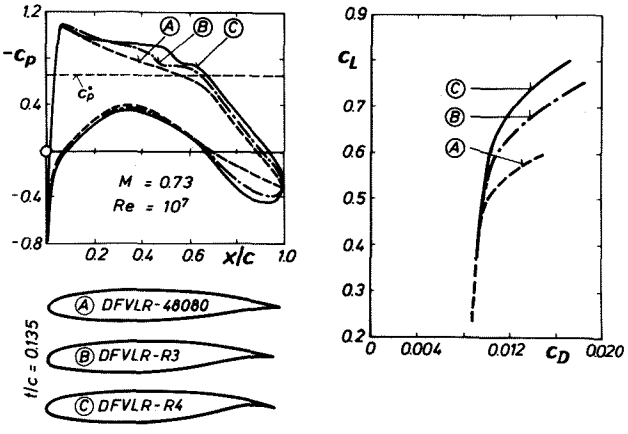

Fig. 3 Development of the transonic airfoil DFVLR-R4

The basic aircraft configuration to be considered was the AIRBUS A310. Fig. 3 shows the development of the airfoils. Starting point was a shockfree airfoil DFVLR-48080 designed by Sobieczky's hodograph method [15]. The shockfree pressure distribution for the Mach number M = 0.73 is shown as case Ⓐ. Unfortunately the lift coefficient of c_L = 0.5 was to low as wing requirements changed. Therefore the airfoil contour had to be modified in the direction of gaining more lift. This procedure seems to be more promising as to design a complete new airfoil. By carefully introducing rear-loading step by step the cases Ⓑ and Ⓒ in pressure distribution were achieved corresponding to lift

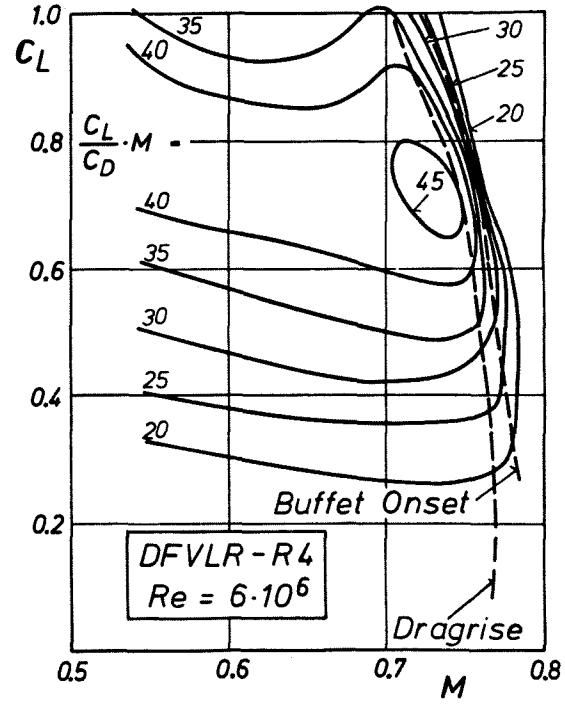

Fig. 4 Measured aerodynamic efficiency of the airfoil DFVLR-R4

coefficients of c_L = 0.6 respectively c_L = 0.65. It is shown that by modifying the lower surface the upper surface pressure distribution is changed, too, by increasing slightly the supersonic region. The calculated drag polars for the cases Ⓐ to Ⓒ indicate that the increase in lift has been achieved without creating additional drag [16]. The airfoil from case Ⓒ named DFVLR-R4 was chosen as candidate airfoil after a lot of off-design calculations have been performed to establish dragrise and buffet onset boundaries. The aerodynamic efficiency of this airfoil measured in the Transonic Windtunnel Braunschweig of DFVLR is shown in Fig. 4 by plotting lines of const. $c_L/c_D \cdot M$ in a lift coefficient Mach number diagram. The highest values of this expression are achieved near the prescribed design condition of c_L = 0.65 and M = 0.73. Also presented in Fig. 4 are the experimentally derived dragrise and buffet onset boundaries.

On the basis of this airfoil a wing design has been performed the results of which have been discussed in [16]. These results indicate, although the design requirements have been fulfilled, further improvements for the wing section seem to be necessary because measured pressure distributions on the wing show the presence of a small zone of separated flow near the trailing edge which could not be detected on the airfoil itself. This effect was attributed to the very large pressure difference near the trailing edge in-

troduced by the rear-loading which probably forces the flow to go around the trailing edge [17]. In order to overcome this problem the pressure distribution of the lower surface was changed as presented in Fig. 5, where the calculated c_p-distributions of the original DFVLR-R4 and the improved airfoil DFVLR-R4/4 are compared at $c_L = 0.6$.

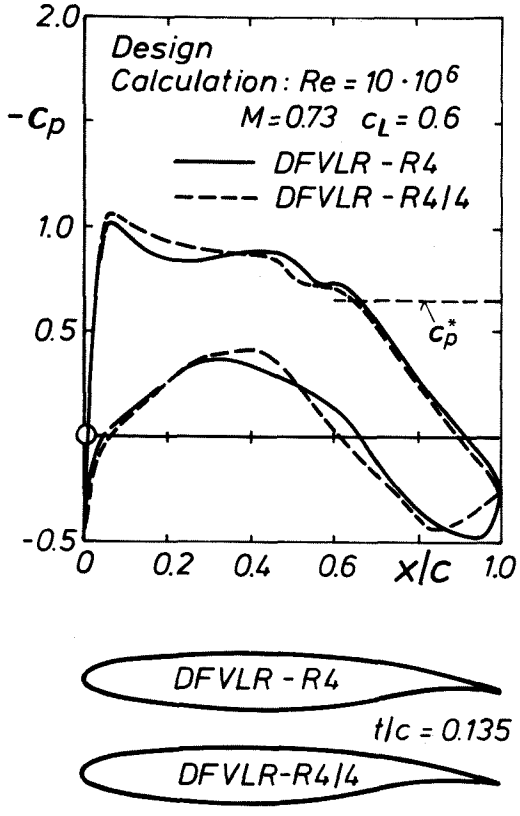

Fig. 5 Design calculation of modified airfoil DFVLR-R4/4

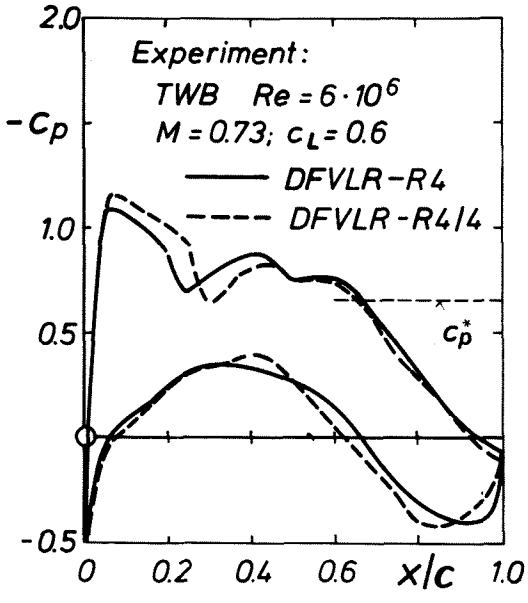

Fig. 6 Comparison of measured pressure distributions of airfoil DFVLR-R4 and R4/4

By properly changing the airfoil contour as indicated in the figure the maximum pressure of the rear-loading is shifted from x/c = 0.95 to x/c = 0.85. The influence on the upper surface pressure distribution is small. For the new airfoil a slightly higher suction level is achieved. Measured pressure distributions at the same condition as presented in Fig. 5 are given in Fig. 6. The predicted modifications by the calculation in surface pressure is confirmed by the experiments. The influence of this modification on the aerodynamic characteristics is presented in Fig. 7 where measured drag polars for M = 0.73 and measured dragrise boundaries of the airfoils DFVLR-R4 and R4/4 are compared. The new airfoil has a lower drag throughout the whole polar and shows a favourable dragrise boundary. The expected good behaviour of the airfoil DFVLR-R4/4 in a wing design has not yet been verified by experiments.

A large amount of fuel can be saved if a laminar boundary layer can be maintained over a great portion of the wing surface. Investigations and experiments have been discussed to a great extent in [18, 19] where suction is applied to stabilize the laminar boundary layer. Although some experiments showed that a remarkable drag reduction could be achieved the concept of suction is very complicated from the viewpoint of handling, manufacturing and controlling. Therefore the possibility of maintaining a laminar boundary layer by applying properly shaped airfoils also at high Reynolds numbers has been investigated [20]. This concept is successfully used since more than twenty years for sailplanes which will be discussed later. Fig. 8 shows a design example for a transport aircraft type airfoil for a high Reynolds number of $Re = 25 \cdot 10^6$. Due to this high Re-number long laminar boundary layers on the airfoil surface can only be obtained if a special type of pressure distribution as shown here is used on upper and lower surface. The flow is accelerating on both sides up to 60% of airfoil chord and then a recompression to free stream condition is followed with such a type of adverse pressure gra-

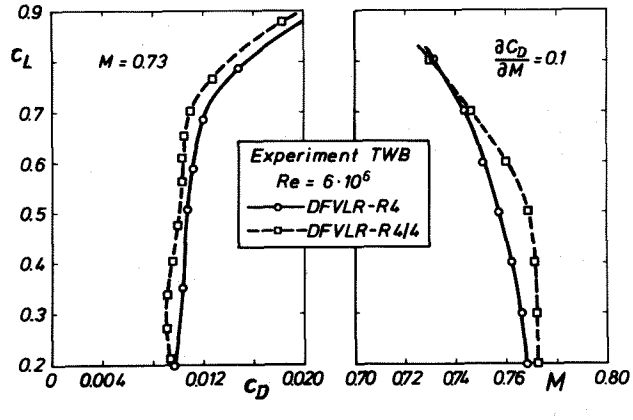

Fig. 7 Drag polars and dragrise boundaries of airfoils DFVLR-R4 and R4/4

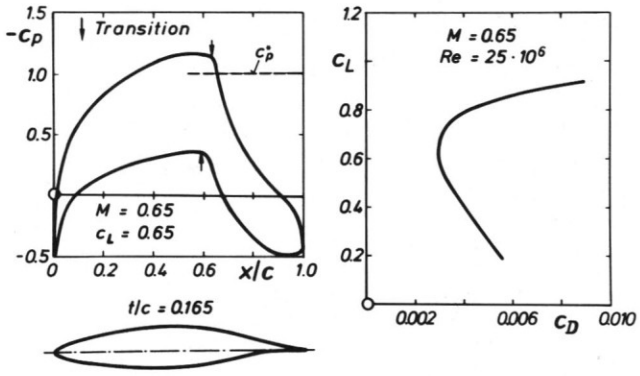

Fig. 8 Drag polar and pressure distribution of a laminar airfoil for a subsonic transport aircraft

dient that turbulent separation is avoided. Transition is calculated to occur at that Re-number at 63% on the upper and at 59% on the lower surface. The resulting airfoil has a thickness ratio of t/c = 0.165 due to the special type of pressure distribution. In order not to run into difficulties with high Mach numbers in the supersonic region leading to strong shock waves the free stream Mach number has to be reduced as for this example to M = 0.65. The achieved lift coefficient for this case is c_L = 0.65. The calculated drag polar for this airfoil shows a remarkably low drag coefficient of c_D = 0.003 in the region near the design point. Beside this region the pressure distribution is changed in that way that transition from laminar to turbulent boundary layer occurs further upstream increasing the drag at low c_L as well as at higher c_L-values.

An experimental proof of such type of pressure distributions has not yet been established. Several problems have to be solved before laminar airfoils for high Reynolds numbers can be used in aircraft projects:

- behaviour of laminar boundary layer on swept wings (flow at the leading edge, crossflow instability),
- influence of airfoil contamination in the normal airline service,
- new concepts for high lift systems without leading edge slats.

4. Sailplanes

Whereas for subsonic transports the laminar flow concept is a subject which still needs intensive research and development before an introduction in practical application can be contemplated, sailplane aerodynamics is a field, where the laminar concept has found a wide application. This is especially due to the relatively moderate Reynolds number which allows laminar flow over a substantial part of the airfoil if the static pressure along the contour is developing in a specific manner. This laminar behaviour has been found for the airfoils of the NACA 6 series and has been exploited by Wortmann [21] and Eppler [22], bringing down the airfoil drag to c_D = 0.005.

When designing airfoils for sailplanes three design conditions have to be taken into account:

- circular climb at low speed
  $c_L \approx 1.0 \div 1.4$ $V_\infty \approx 70 \div 80$ km/h
- distance flight at high speed
  $c_L \approx 0.2 \div 0.3$ $V_\infty \approx 130 \div 200$ km/h
- flight at best glide angle
  $c_L \approx 0.8$ $V_\infty \approx 100$ km/h.

A useful airfoil for a sailplane has a large extent of laminar flow for all these conditions (upper side x/c ≈ 0.6, lower side x/c ≈ 0.7). For the Reynolds numbers which occur on sailplanes ($1 \cdot 10^6 \leq Re \leq 4 \cdot 10^6$) these long laminar boundary layers end in a separation bubble of sometimes considerable extent generating additional drag and so perturbating the laminar flow concept.

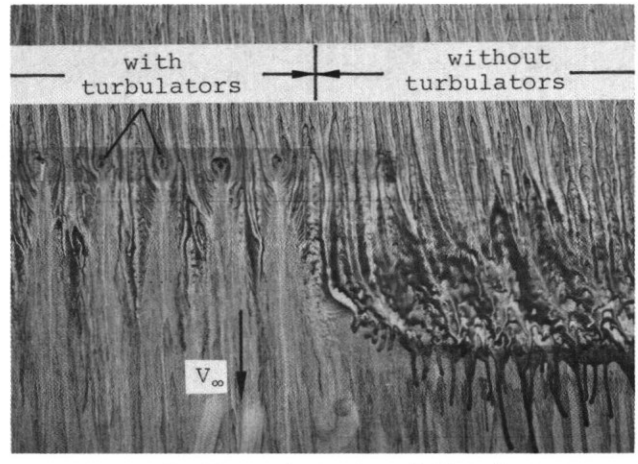

Fig. 9 Oil flow picture of the lower surface of a sailplane showing the effect of pneumatic turbulators

At DFVLR a method has been found to avoid separation bubbles in order to get full benefit of the laminar option [23], [24]. The basic idea is to produce a flow distortion just in front or inside of the laminar separation bubble. Vortex generators or fences seem not to be adequate devices since they generate additional drag for off-design cases. The solution presented here are pneumatic turbulators. By blowing air of higher pressure out of small holes into the critical region laminar separation bubbles can be avoided. Fig. 9 shows the effect of a row of small jets on the flow field. What can be seen is the lower part of a wing, with visualization of the flow by oil: without blowing a separation bubble occurs; with blowing the laminar boundary layer transits immediately behind the row from

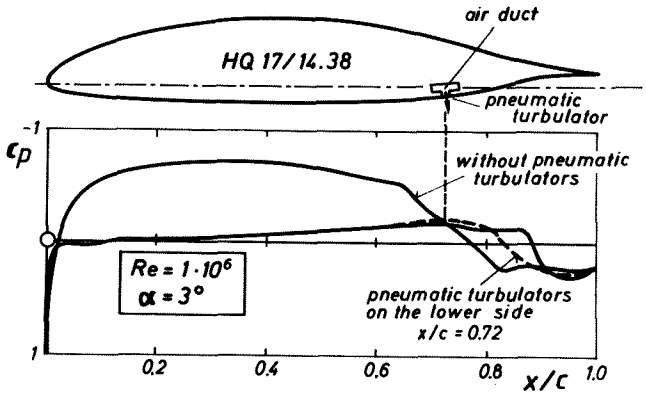

Fig. 10 Effect of pneumatic turbulators on the pressure distribution of the airfoil DFVLR-HQ17

laminar to turbulent. This flow visualization has been achieved on a sailplane with a modified wing in order to investigate the effect of blowing in flight. The foto gives an impression of the very small size of the holes (0.4 mm diameter) and the relatively wide distance from one to another. The amount of blowing necessary to achieve this effect is rather small ($c_Q \approx 5 \cdot 10^{-6}$) and has no effect on the overall drag.

Fig. 10 shows the airfoil DFVLR-HQ17, designed to have long laminar boundary layers on upper and lower side. Whereas the upper side has a small bubble which has no dominant influence on the airfoil drag, at the lower side a rather long bubble occurs which can be destroyed by blowing at the location x/c = 0.72. The overall influence on the drag is given in Fig. 11, where results from the laminar windtunnel of the Technical University Delft are given. The drag reduction by blowing achieved is about 15% over a large range of c_L and leads to a minimum drag of 0.0042 for an airfoil of 14% relative thickness.

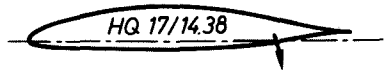

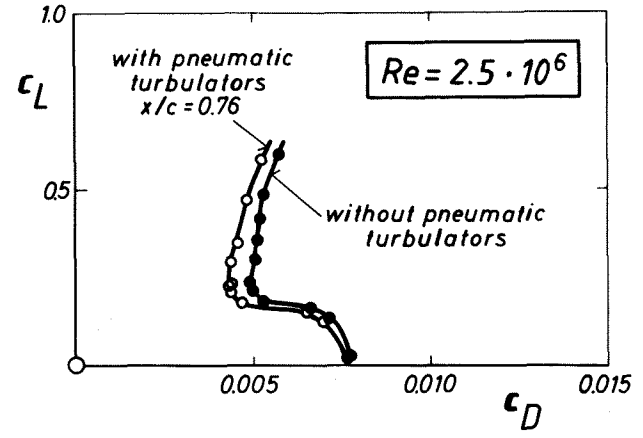

Fig. 11 Effect of pneumatic turbulators on the drag polars of the airfoil DFVLR-HQ17

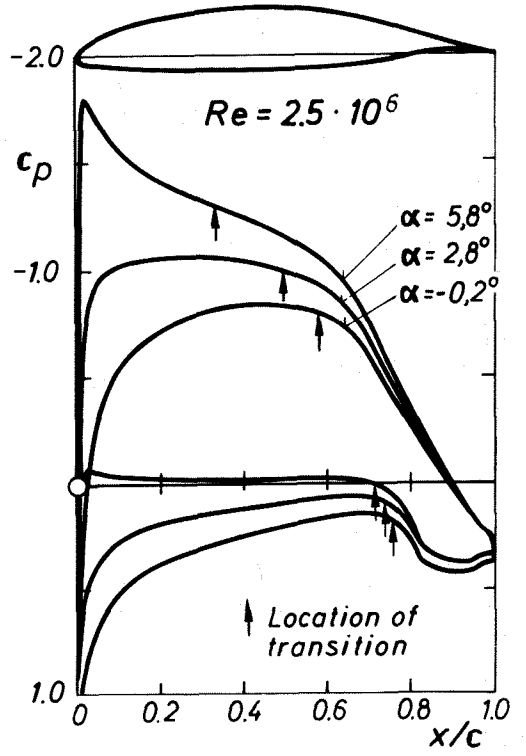

Fig. 12 Pressure distributions of the laminar airfoil DFVLR-HQ17 at several angles of attack α

The use of blowing turbulators, as described here, requires a rather stable length of the laminar boundary layer for a large range of α-Re combinations, since a blowing device can only be attached at a fixed place. This cannot be achieved on the upper side, since the pressure distribution varies with angle of incidence quite strongly (Fig. 12). Here the pressure distribution should be chosen in such a way, that a destabilization region leads to a natural transition. On the lower side a long pressure plateau can be achieved with laminar flow up to x/c = 0.7 ÷ 0.8 for a large range of angles of attack. Here a blowing device is favorable to avoid a bubble.

The airfoil just described has been incorporated in the new sailplane ASW-22 (Fig. 13), which shows an excellent performance. The air, which is necessary for blowing, is kept by a probe in the stagnation region of the wing-root. This airfoil is one of a number of airfoil designs, the so-called DFVLR-HQ (Horstmann, Quast) airfoils. Most of these designs have been done with the Eppler/Somers method for airfoils with blowing and airfoils with natural destabilization and comprise clean airfoils, airfoils with camber flap and airfoils with extended flap.

Airfoils with extended flap are especially suited to meet the very different requirements of low and high speed flight [25]. Fig. 14 shows results for such an

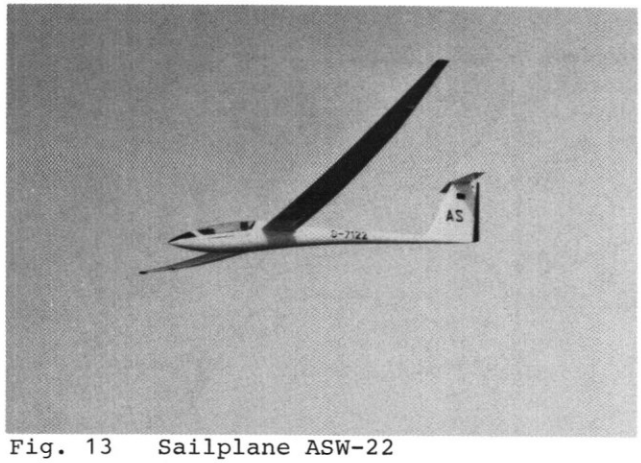

Fig. 13 Sailplane ASW-22

airfoil. The drag polars show that with this design the different design requirements of a sailplane can be matched in a convenient way. The results given here have been achieved with the flying testbed. The airfoil developed then has been used within the design of the sailplane SB-11 of the "Akademische Fliegergruppe (AKAFLIEG) Braunschweig". With this sailplane H. Reichmann won the world championship in 1978.

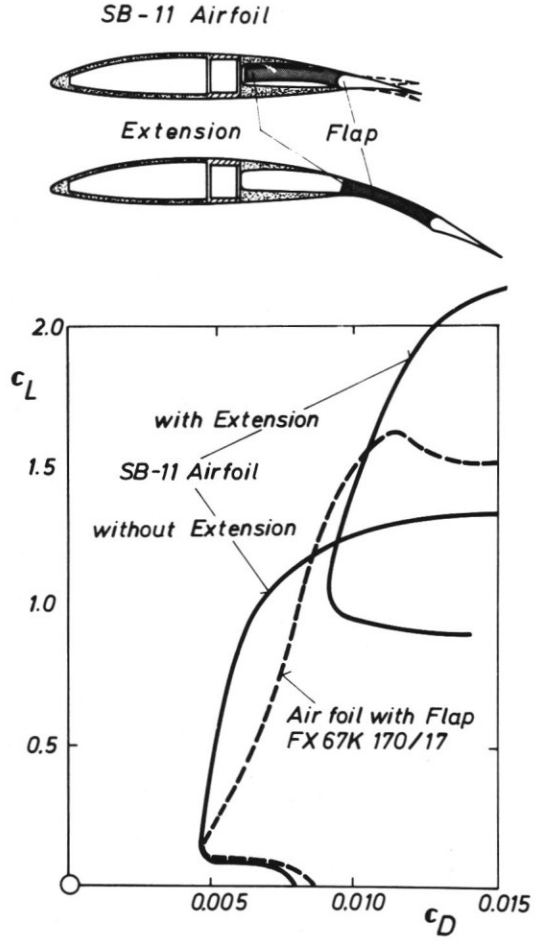

Fig. 14 Drag polars of the airfoil with extended flap of the sailplane SB-11

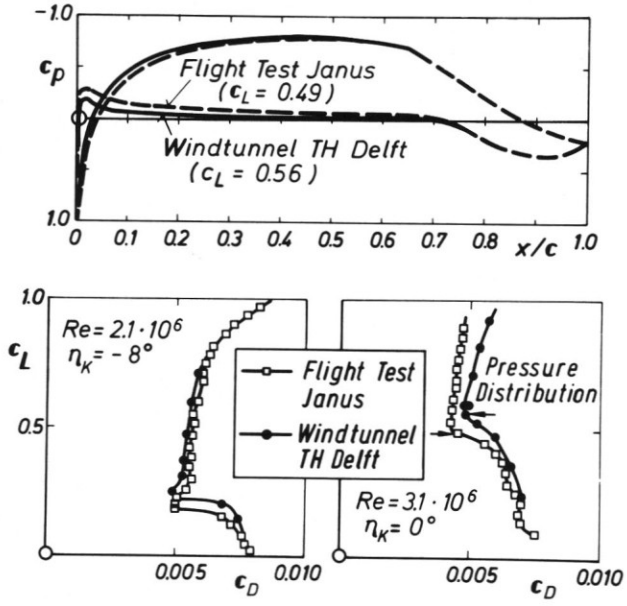

Fig. 15 Comparison of windtunnel and flight test for the airfoil DFVLR-HQ17

One of the main problems of windtunnel testing of laminar airfoils is the turbulence problem. With the flying testbed it is possible to compare windtunnel and free flight. Fig. 15 presents the drag polars for two flap deflections resp. Reynolds numbers. Comparing the drag level it can be seen that for Re = 2.1 · 10^6 the flight tests indicate a higher drag than the windtunnel tests. This is due to a larger separation bubble on the lower surface in free flight conditions creating more drag. For the higher Re-number Re = 3.1 · 10^6 the drag level for the flight tests is much lower compared to the windtunnel tests. This is due to a longer laminar boundary layer on the upper surface in the flight experiments. In the windtunnel tests the transition from laminar to turbulent boundary layer occurs further upstream than in free flight. Furthermore it can be seen that the region of low drag extends to lower lift coefficients in flight. This behaviour can be explained by the pressure distributions at the kink points for Re = = 3.1 · 10^6 marked in the drag polars. Important here is the long laminar boundary layer on the lower surface (up to 70% chord) which for the free flight conditions (low turbulence) can tolerate a steeper pressure gradient leading to a lower lift coefficient with low drag.

These examples show that the laminar option is an exciting feature and exhibits interesting prospects. Furthermore research on sailplane aerodynamics has a large impact on the development of airfoils for other types of aircraft.

5. Propeller and helicopter blades

Propellers for General Aviation aircraft now in use can be improved substantially. Compared to maximum theoretical thrust after momentum theory static thrust coefficients of 50% to 70% and cruise thrust coefficients of 90% are attainable. Thus with proper means especially during take-off and climbing remarkable improvements in thrust can be expected. Reductions of take-off field length and noise annoyance of airfield neighbours are then a favourable consequence. Furthermore for twin engine aircraft the payload can be increased due to increased take-off weight being not restricted during one engine climb.

In co-operation with "DORNIER" and "Propeller Hoffmann" in the Civil Component Programme (ZKP) "Improved Propellers for General Aviation Aircraft" [26] four airfoils for a variable pitch propeller of 750 PS power have been designed. The four blade sections DFVLR-P1 to DFVLR-P4 correspond to different locations on the blade. As the maximum thrust coefficients on a propeller blade are normally reached at 80% of blade radius this section is of prime interest and further discussions will concentrate on this specific section.

Starting from the requirements of the propeller the airfoil design specifications

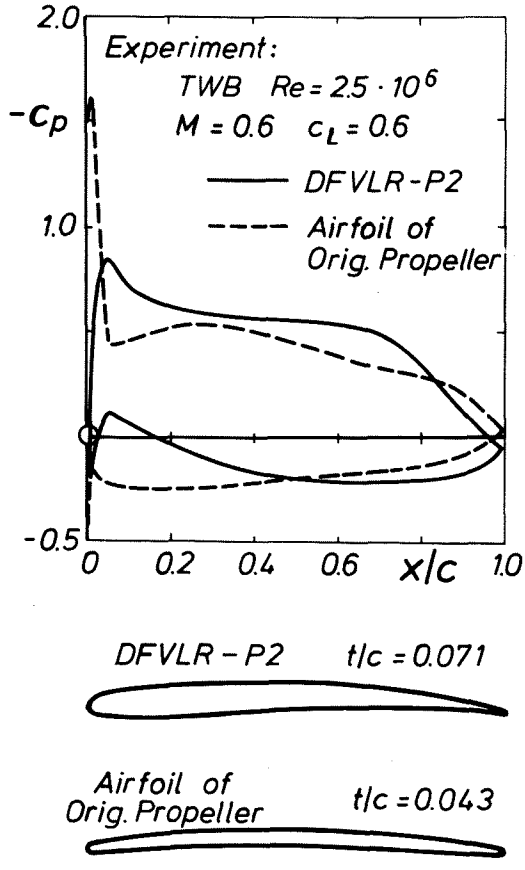

Fig. 16 Comparison of pressure distributions of two propeller blade sections

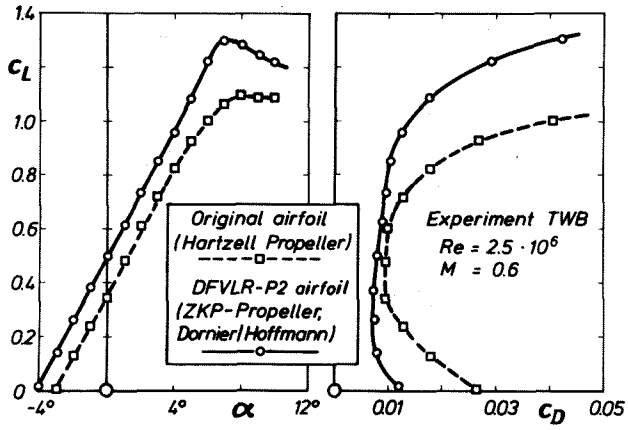

Fig. 17 Comparison of lift curves and drag polars for two propeller blade sections

can be derived as follows:

- high maximum lift coefficient at low Mach numbers M = 0.4 to 0.5 for high static thrust at take-off condition,
- high lift/drag ratio c_L/c_D at M = 0.6 and c_L = 0.6 to encounter the climb conditions,
- low drag coefficients at low lift coefficients of $c_L \leq 0.4$ at higher Mach numbers M ≈ 0.7 to avoid performance loss during cruise flight,
- as the blades of the new propeller should be manufactured from composites the relative thickness of the airfoil compared to conventional aluminium alloy propellers has to be increased and nearly doubled.

The last demand for higher thickness ratio normally leads to increased minimum drag coefficients. In order to compete with conventional thin sections in this respect new ideas concerning laminar boundary layers have to be taken into account when designing the new airfoils. Here the experience achieved with laminar airfoils for sailplanes is of major importance (Chapter 4).

Fig. 16 shows the shape and the measured pressure distribution of the new airfoil DFVLR-P2 designed with the method described in [6], for the Mach number M = 0.6 at a lift coefficient of c_L = 0.6 at a Reynolds number of Re = 2.5 · 10^6 [27]. The airfoil has a thickness ratio of t/c = 0.071. The pressure distribution demonstrates the design concept. Both upper and lower surface pressure only show small suction peaks followed by a smooth variation of pressure. For this case a laminar boundary layer on the upper surface is expected up to 50% of airfoil chord whereas on the lower surface transition may occur at 20% to 30% of chord. At higher angles of attack the suction peak on the upper surface increases and transition moves forward to the leading edge. On

the lower surface the suction peak will vanish and a long laminar boundary layer is obtained. For lower lift coefficients the pressure peak on the upper surface vanishes and transition is expected to occur at 65% of airfoil chord whereas the lower surface will have a suction peak causing a turbulent boundary layer near the leading edge. The design idea is to have at the different design conditions stated above at least on one surface a long laminar boundary layer. Due to the moderate thickness of the blade section it seems to be impossible to achieve this on both surfaces as it is known from sailplane airfoils.

Furthermore Fig. 16 presents the measured pressure distribution of a comparable blade section of a propeller of usual standard [28]. This section has a thickness of t/c = 0.04 and shows high suction peaks on both surfaces for the same flow conditions as the new section. These peaks will lead to flow separation near the leading edge creating also unfavourable acoustic effects. Thus with the new section DFVLR-P2 aerodynamic as well as acoustic advantages are expected. This is demonstrated at least for the aerodynamic behaviour in Fig. 17 where the lift coefficients c_L vers. angle of attack α and the drag polars c_L vers. c_D of the airfoil DFVLR-P2 are plotted together with the corresponding values of the blade section of usual standard. The new airfoil DFVLR-P2 has a higher maximum lift c_{Lmax} and a lower drag coefficient at all angles of attack. This holds not only for the Mach number M = 0.6 as indicated in this figure but also for lower and higher Mach numbers although the relative thickness of the new section is 80% higher compared to the thickness of the propeller of usual standard.

With this new airfoil DFVLR-P2 together with the other ones DFVLR-P1, P3 and P4 a new propeller – called "ZKP-Propeller" – has been designed by DORNIER and manufactured by Propeller-Hoffmann [26]. Model tests at DFVLR Göttingen and full-scale flight tests on the TNT-Experimental Aircraft (Fig. 18) from DORNIER [29] confirm the good characteristics of the airfoils

Fig. 18 DORNIER TNT experimental aircraft with ZKP-propeller

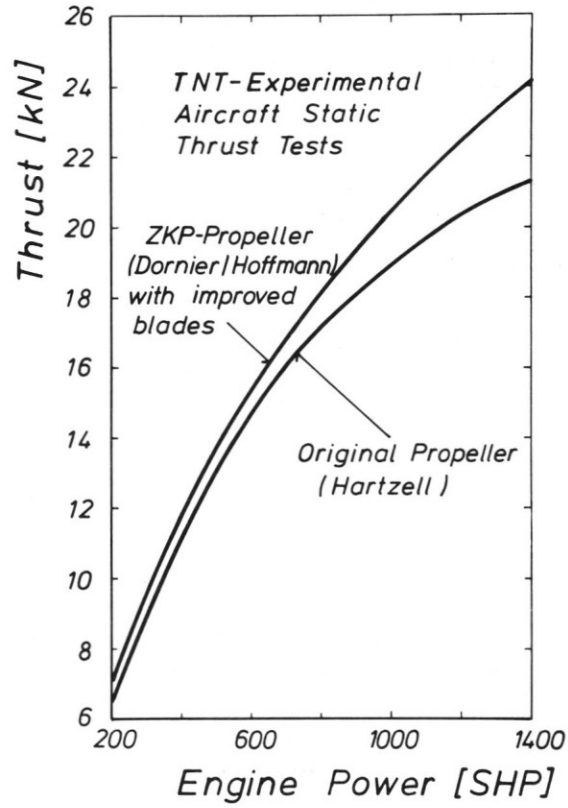

Fig. 19 Comparison of static thrust of TNT experimental aircraft with two different propellers

also for the propeller [30]. This is true not only for the aerodynamics but also for the acoustic behaviour. Fig. 19 presents results of recent full scale static thrust tests on the TNT-Experimental Aircraft for the ZKP-Propeller with the new blade sections and the propeller of usual standard. This figure clearly indicates that the static thrust is increased by nearly 15%. During climb (one engine and two engine climb) the performance of the ZKP-Propeller was also improved. No loss in performance but also a slight improvement was obtained in cruise flight. In addition the noise radiation of the ZKP-Propeller was less or equal to that of the propeller of usual standard although the blade thickness was nearly doubled.

With the permanent demand of improving the performance of modern helicopters, the requirements of their aerodynamic characteristics have increased. Beside the reduction of parasite drag of the helicopter as a whole the aerodynamic design of the rotor is of great importance. The rotor itself is not only influencing the performance with its aerodynamic behaviour but it imposes real aerodynamic limitations to the flight envelope. These limitations are due to Mach number effects on the advancing blade and due to stall effects on the retreating blade. In order to extend the flight envelope of the helicopter, improvements in rotor aerodynamics are necessary

which mainly depend on the blade sections [31, 32].

The design objectives for a blade section can be deduced from the inspection of the operating conditions of the helicopter blade during one cycle for different flight conditions as cruise flight, hovering and manoeuvre flight. Thus the following design specifications for an outboard section of a helicopter rotor (75% to 90% of blade span) can be derived:

- high drag divergence Mach number $M_D \approx 0.8$ to 0.84 for lift coefficients near $c_L \approx 0$ and small pitching moment coefficients $c_m \leq |0.01|$ for encountering the cruise flight conditions,
- high lift/drag ratios at M = 0.6 and moderate lift coefficients $c_L \approx 0.5$ to 0.6 for hovering and cruise flight,
- high maximum lift coefficients $c_{Lmax} \approx 1.5$ to 1.3 in the Mach number range M ≈ 0.3 to 0.5 for the manoeuvre flight,
- additional geometrical constraints for the blade sections are introduced due to structural demands requiring a sufficient torsional stiffness and a satisfying structural strength. This leads to blade section thicknesses of:

  t/c ≈ 0.12 up to 80% of blade span

  t/c ≈ 0.09 from 80% to 90% of blade span

  t/c ≈ 0.07 at the tip station.

According to this design specifications two airfoils of 9% and 12% thickness have been developed in co-operation with MBB. In order to encounter the low drag requirements for the advancing blade at high Mach numbers and the high lift/drag ratio at M = 0.6 also here laminar boundary layer concept was incorporated in the design process. Flow visualization tests on a helicopter rotor of a Bo 105 helicopter indicated that laminar boundary layers of moderate length appeared also on the upper surface of the blade during hovering flight, although no care was undertaken to have a very clean and smooth blade surface. The rotating flow field seems to have a stabilizing effect on the boundary layer.

Fig. 20 presents the two airfoils DM-H1 of t/c = 0.09 corresponding to a blade station of approximately 90% of the blade span and DM-H2 of t/c = 0.12 for a blade station of 80% of span. The aerodynamic behaviour at the Mach number M = 0.6 is exemplary given by the measured drag polars at $Re = 4.8 \cdot 10^6$ from the Transonic Windtunnel Braunschweig (TWB). For the airfoil H1 minimum drag coefficients of $c_D \approx 0.0072$ respectively $c_D \approx 0.0078$ for the airfoil H2 are measured. Due to the greater thickness the airfoil H2 has a higher drag level but compared to airfoil H1 the low drag values

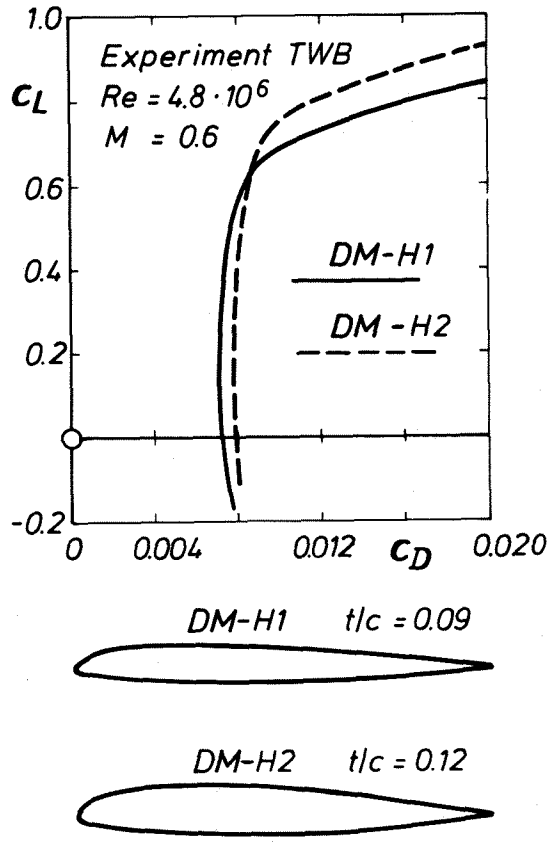

Fig. 20 Drag polars for the helicopter blade sections DM-H1 and DM-H2

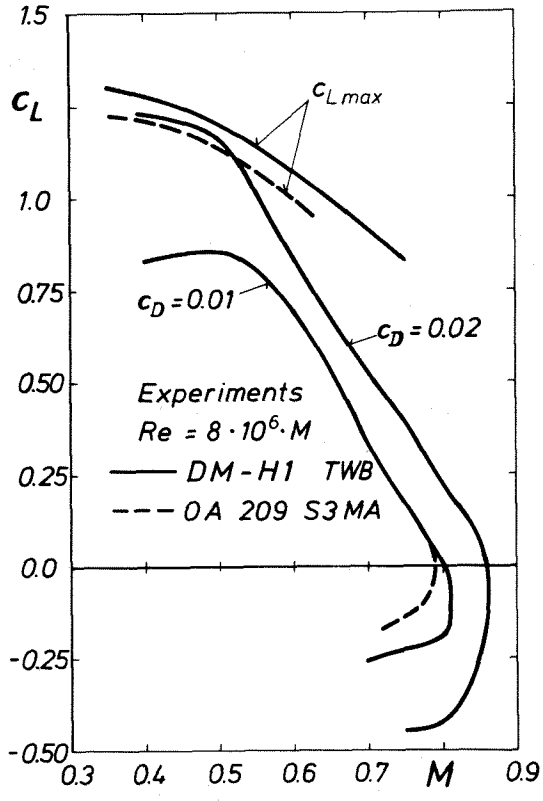

Fig. 21 Measured performance boundaries of the airfoil DM-H1

extends to higher lift coefficients. In the region of $c_L \approx 0.6$ lift/drag ratios of $c_L/c_D \approx 75$ are achieved. The aerodynamic performance of the airfoil H1 is summarized in Fig. 21 in a lift coefficient vers. Mach number diagram presenting the maximum lift coefficient and the drag divergence Mach number M_D boundaries as measured in the TWB at $Re = 8 \cdot 10^6 \cdot M$. M_D is here determined by a constant drag level of $c_D = 0.01$ respectively $c_D = 0.02$. c_{Lmax} values of 1.3 at $M = 0.4$ are achieved and the drag divergence Mach number M_D at $c_L \approx 0$ is M_D ($c_D = 0.02$) = 0.86. Comparable curves for the modern helicopter airfoil OA209 as measured in the ONERA S3MA windtunnel [33] for maximum lift and M_D ($c_D = 0.01$) are also presented in this figure. It is shown that DM-H1 airfoil has a slightly better performance.

Fig. 22 presents the boundaries for the DM-H2 airfoil in comparison with the prediction from the design methods as discussed in section 2 of this paper. For this thicker airfoil c_{Lmax} values of 1.5 at $M = 0.3$ are achieved, which is in good agreement with the calculations. Drag divergence Mach numbers of M_D ($c_D = 0.01$) = = 0.8 and M_D ($c_D = 0.02$) = 0.84 were measured at $c_L \approx 0$. The calculations show slightly smaller values. All in all the predictions of the airfoil performance are in satisfactory agreement with the measured values.

The pitching moment behaviour of the H1 airfoil is presented in Fig. 23 against Mach number for different constant lift coefficients of $c_L = 0.0$ to $c_L = 0.6$. The measurements clearly indicate that the requirements of $c_m \leq |0.01|$ are fulfilled up to high Mach numbers where then a steep increase in nosedown pitching moment occurs.

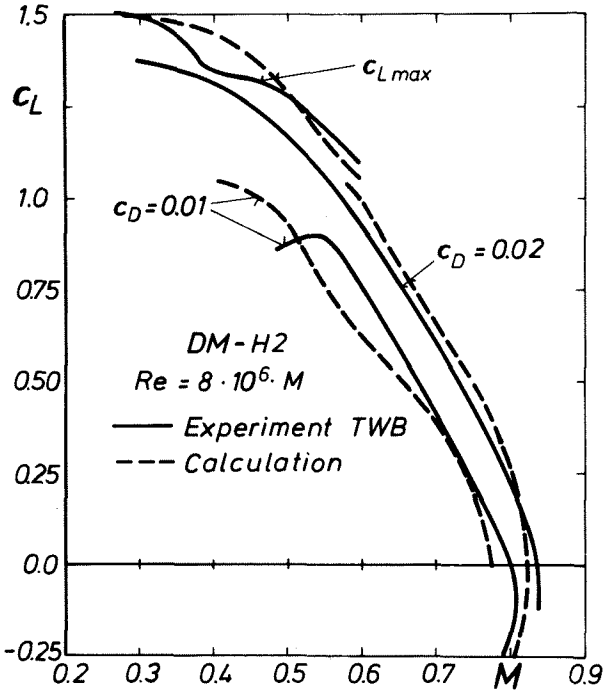

Fig. 22 Comparison of calculated and measured performance boundaries of the airfoil DM-H2

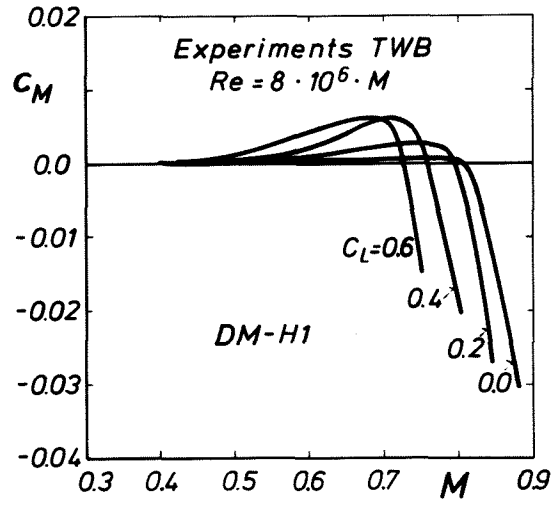

Fig. 23 Pitching moment coefficients vers. Mach number of the airfoil DM-H1

With these performance data shown here a new helicopter rotor can be designed giving a remarkable improvement compared with rotors having usual NACA airfoils.

6. Combat aircraft

When looking at combat aircraft several design requirements have to be taken into account. The most important of these are

- low c_L and low c_D at high supersonic Mach numbers ($M \approx 1.3 \div 2.0$),
- moderate c_L and low c_D at high subsonic Mach numbers ($M \approx 0.7 \div 1.0$) for subsonic/transonic cruise condition,
- high c_L and moderate c_D at subsonic manoeuvre flight ($M \approx 0.6 \div 0.9$),
- high c_L and high c_L/c_D at low speed for take-off
- very high c_L at low speed for landing.

Option 1 and 2 require thin uncambered airfoils ($0.03 \leq t/c \leq 0.06$) whereas the options 3 ÷ 5 can be fulfilled by flap setting or variable camber. The discussion within this chapter mainly concentrates on option 2 well having in mind the others*.

The application of a laminar option seems not to be adequate for this design task but advanced transonic design might

* This study has been funded by the Ministry of Defense.

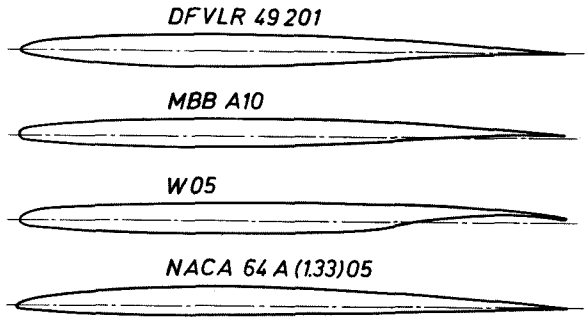

Fig. 24 Shapes of the investigated four airfoils

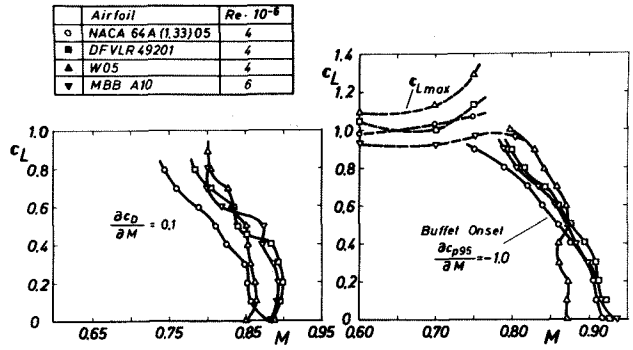

Fig. 25 Dragrise and buffet onset boundaries of four thin airfoils

generate substantial improvements. Therefore the key question investigated here is whether an advanced transonic design brings an improvement against conventional airfoils. This question is not a trivial one, because with descreasing thickness the possibilities of airfoil modification are reduced. In order to answer this question, three advanced airfoils have been compared with a conventional one, all having the same relative thickness of t/c = 0.05 [34].

All airfoils are shown in Fig. 24. The transonic airfoil DFVLR 49201 has been designed by Sobieczky with a hodograph method [10]. For this airfoil a supersonic slopy roof-top on the upper side of the airfoil was aimed at. The same is with the MBB A10, which has been designed by Eberle with a somewhat different hodograph method [35]. In contrast to DFVLR 49201 MBB A10 has a bluff nose, a certain amount of rear-loading and a bit higher thickness (t/c = 0.054). The third advanced airfoils is the W05 which has been designed by Eberle following Whitcomb's guidelines for supercritical airfoil design [36]. This airfoil has a flat upper surface and a large camber in the rear part, which leads to an extended supersonic roof-top and a considerable rear-loading.

These three transonic airfoils having different design philosophy are compared with the NACA 64A(1.33)05, a conventional airfoil which has been used for a number of investigations on wings in the MBB-AVA-Pilot-Model.

Of great importance for aircraft performance are drag-rise, buffet onset and c_{Lmax} which will be analysed first. The drag-rise, given in Fig. 25, indicates quite clearly the superiority of an advanced transonic design against a conventional one. It can be seen that in the region $0.1 \leq c_L \leq 0.5$ DFVLR 49201 has a gain of $\Delta M \approx 0.04$. MBB A10 behaves similar whereas W05 is worse in the region which is due to supersonic flow with shocks on the lower side. At higher lift coefficients ($c_L \geq 0.6$) W05 shows a better performance than all other airfoils investigated.

This demonstrates quite clearly that, depending on the rear-loading the region of best performance occurs either at low or high lift coefficients. For a practical airfoil design it seems reasonable to choose a basic airfoil without rear-loading which matches the requirements for subsonic cruise and supersonic flight and to get the required additional lift in manoeuvre conditions by flap-deflection or variable camber.

As to buffet onset, it can be seen, that by transonic design concept only small improvements can be achieved. For DFVLR 49201 and MBB A10 the gains are $\Delta M \approx 0.01 \div 0.02$. For W05 at low lift coefficients $0 \leq c_L \leq 0.5$ there is even a deterioration up to $\Delta M \approx -0.05$; for high values of c_L nevertheless an important improvement of $\Delta M \approx 0.04$ can be achieved. This again is due to the extreme rear-loading of this airfoil.

The maximum lift could only by evaluated for Mach numbers below M = 0.75. The highest maximum lift is given – as expected – by W05. Remarkable is the low c_{Lmax}-value of MBB A10. This results from the very bluff nose of the airfoil with two curvature maxima above and below the nose point, which obviously leads to premature separation.

As can be seen rear camber has an important influence on airfoil performance and can be used to match quite different flight requirements. To get a better insight into camber effects the NACA 64A(1.33)05 has been equipped with flaps [37]. In Fig. 26 the clean airfoil is compared with a configuration with a trailing edge flap deflection of 5^o. The factor $c_L/c_D \cdot M$ which is a good indicator of the aerodynamic efficiency is given in a c_L-M-diagram. The experimental results show that the clean airfoil has a maximum value of 45, which lies in the region $0.75 \leq M \leq 0.8$ and $c_L \approx 0.5$. With a flap deflection of 5^o a substantial improvement to a value of more than 50 can be achieved over a range $0.7 \leq M \leq 0.8$ and $0.5 \leq c_L \leq 0.8$. The maximum value is 60 at M = 0.75 and $c_L = 0.8$.

The drag-rise curve – also given in this diagram – shows the same tendency found in

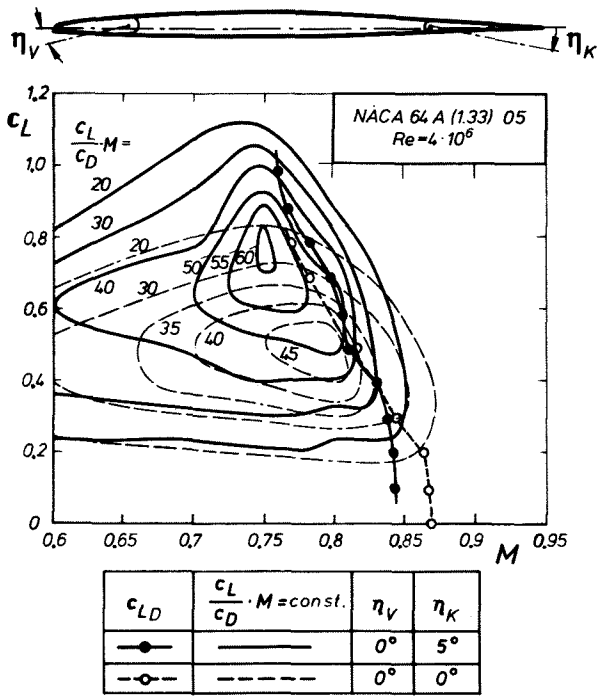

Fig. 26 Influence of flap deflection on the aerodynamic efficiency of the airfoil NACA 64A(1.33)05

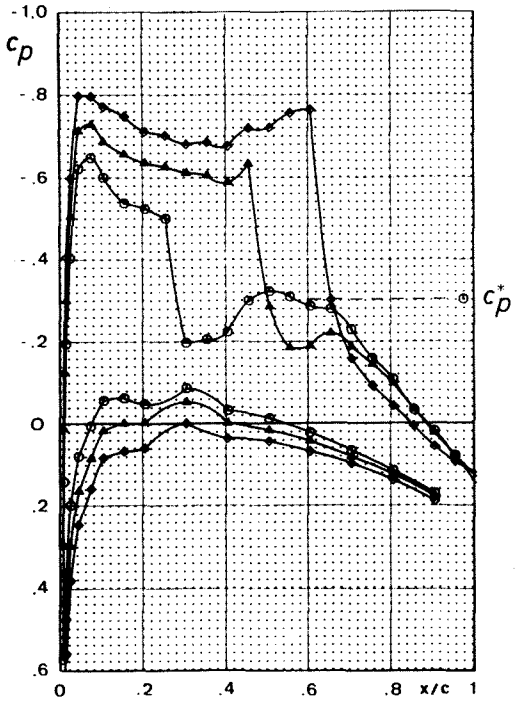

Nr.	M	Re·10⁻⁶	Alpha [°]	c_L	c_M	c_D
⊙ 3474	0.850	4.05	1.00	0.300	-0.0403	0.00682
▲ 3475	0.851	3.92	1.50	0.414	-0.0405	0.00872
◆ 3476	0.849	3.95	2.00	0.560	-0.0615	0.01843

Fig. 27 Pressure distributions of the airfoil DFVLR 49201 at M = 0.85

Fig. 25 comparing DFVLR 49201 and WO5: for low lift coefficients the clean airfoil has advantages whereas beyond c_L = 0.5 this is vice versa.

For a better analysis of the results achieved, some specific pressure distributions of the airfoils DFVLR 49201 and WO5 for the region of design condition M = 0.85 c_L = 0.3 ÷ 0.7 shall be discussed. Fig. 27 shows that for DFVLR 49201 a slopy roof-top pressure distribution on the upper side is achieved which ends in a weak shock. A small amount of lift is generated by a weak rear-loading. Increasing the angle of attack leads to a supersonic roof-top pressure distribution which ends with a shock. Further increase in angle of attack generates trailing edge flow separation, which occurs at a lift coefficient of 0.75.

Fig. 28 shows the development of the pressure distribution of WO5 which has a completely different design philosophy. The main characteristics namely the extended supersonic roof-top and an extremely high loading at the trailing edge can be seen best for c_L = 0.663 and 0.773. The supersonic roof-top extends up to x/c = 0.8 creating high lift coefficients. With decreasing angle of attack the supersonic zone breaks down and two shocks occur on the upper side. Although the first shock is travelling very fast across the flat upper surface with rising or decreasing angle of attack, the pitching moment shows only a moderate change. Furthermore the drag remains low up to a lift coefficient of 0.52. This is obviously due to the sec-

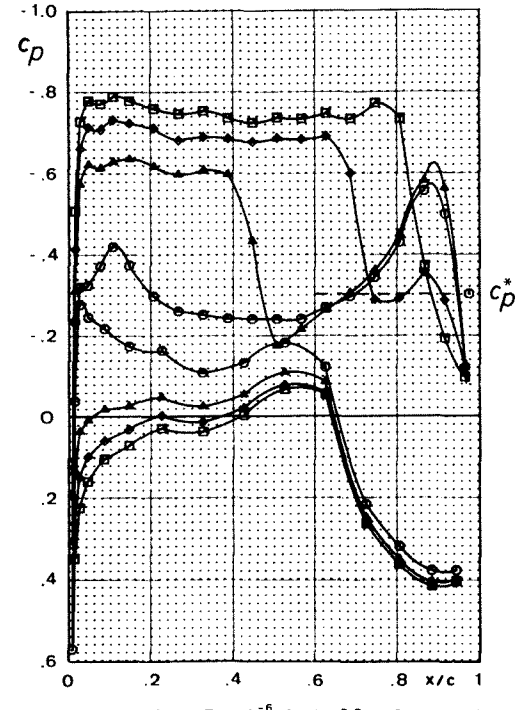

Nr.	M	Re·10⁻⁶	Alpha [°]	c_L	c_M	c_D
⊙ 3757	0.850	3.97	0.00	0.303	-0.1354	0.00770
▲ 3758	0.849	4.02	1.00	0.525	-0.1407	0.00892
◆ 3762	0.849	3.96	1.50	0.663	-0.1498	0.01481
⊡ 3764	0.849	3.98	2.00	0.773	-0.1788	0.01889

Fig. 28 Pressure distributions of the airfoil WO5 at M = 0.85

ond acceleration of the flow behind the first shock which hinders the boundary layer from a premature separation.

The other remarkable point is the extremely high rear-loading. It does not only generate additional lift on the lower side but also on the upper side due to a flap-kink-like peak at approximately x/c = 0.9. Although behind this point a steep pressure rise occurs there is no premature separation. May be, that an incipient separation occurs just in front of the trailing edge – as shown for R4 (see chapter 3).

6. Conclusions

Recent airfoil investigations using the transonic design option and/or the laminar option show that substantial improvements in airfoil performance can be achieved. This is shown for airfoils for subsonic transports, combat aircraft, sailplanes, propellers and helicopter rotors. Summarizing, the subsequent statements can be made:

- transonic design concepts incorporated in thin uncambered airfoils bring a substantial improvement of the drag-rise boundaries,
- alternative philosophies for transonic airfoil design lead to quite different airfoil characteristics,
- changes in the character of rear-loading reduce the drag of thick transonic airfoils,
- use of the laminar option based on proper contouring leads to massive drag reductions at moderate subsonic speeds,
- use of the laminar design option combined with the application of pneumatic turbulators to avoid separation bubbles reduces the drag of airfoils in the Reynolds number region up to $3 \cdot 10^6$,
- extended flaps improve the proper matching of design requirements for sailplanes,
- introduction of partly laminar flow leads to improved airfoils for propellers and rotors.

All these improvements have been achieved due to advanced theoretical methods and improved respectively new experimental techniques in windtunnel and flight. Especially flight tests have got a special importance since the influence of windtunnel-turbulence can be eliminated, which is of special importance for the laminar design option.

Acknowledgements

The authors thank Dipl.-Ing. K.H. Horstmann, Dipl.-Ing. H. Köster, Dipl.-Ing. R. Müller, Dipl.-Ing. W. Puffert-Meißner and Dipl.-Ing. A. Quast from the Institute for Design Aerodynamics of DFVLR for their assistance in preparing this paper.

The companies "Alexander Schleicher, Segelflugzeugbau" and "DORNIER GmbH" are acknowledged for their permission to publish the figures 13, 18 and 19.

References

[1] Pearcey, H.H.: The aerodynamic design of section shapes for swept wings. Advances in Aeron. Sc. 3, Pergamon Press, pp. 277-323 (1962).

[2] Nieuwland, G.Y.: Transonic potential flow around a family of quasi-elliptical sections. NLR TR T-172 (1967).

[3] Whitcomb, R.T.: Review of NASA supercritical airfoils. ICAS Paper 74-10 (1974).

[4] Eppler, R.; Somers, D.M.: A computer program for the design and analysis of low-speed airfoils. NASA TM 80210 (1980).

[5] Walz, A.: Strömungs- und Temperaturgrenzschichten. Braun, Karlsruhe, 1966; translated as: Boundary layers of flow and temperature. MIT. Press, 1969.

[6] Radespiel, R.: Erweiterung eines Profilberechnungsverfahrens im Hinblick auf Entwurfs- und Nachrechnungen von Laminarprofilen bei Verkehrsflugzeugen. DFVLR IB 129-81/15 (1981).

[7] Bauer, F.; Garabedian, P.; Korn, D.; Jameson, A.: Supercritical Wing Sections I, II, III. Lecture Notes in Economics and Mathematical Systems, Vol. 66 (1972), Vol. 108 (1975), Vol. 150 (1977). Springer-Verlag Berlin/Heidelberg/New York.

[8] Jameson, A.: Iterative solution of transonic flow over airfoils and wings, including flows at Mach 1. Communications on Pure and Applied Mathematics, Vol. 27, pp. 283-309 (1974).

[9] Nandanan, M.; Stanewsky, E.; Inger, G.R.: A computational procedure for transonic airfoil flow including a special solution for shock boundary layer interaction. AIAA Paper 80-1389 (1980).

[10] Sobieczky, H.: Related analytical, analog and numerical methods in transonic airfoil design. AIAA Paper 79-1556 (1979).

[11] McFadden, G.B.: An artificial viscosity method for the design of supercritical airfoils. NASA-CR-158840 (1979).

[12] Stanewsky, E.; Puffert-Meißner, W.; Müller, R.; Hoheisel, H.: Der Transsonische Windkanal Braunschweig. DFVLR IB 129-82/1 (1982). Submitted for publication to Z. Flugwiss.

[13] Horstmann, K.H.; Quast, A.; Kunze, U.: Das Segelflugzeug "JANUS" als Versuchsträger für Profilmessungen. 4. Symp. f. Segelflugzeugentwicklung, Stuttgart 1980.

[14] Körner, H.: Entwurf und Windkanalerprobung überkritischer Profile im Rahmen der ZKP-Aufgabe "Flügelsektion". DFVLR IB 151-76/20 (1976).

[15] Sobieczky, H.: Application of generalized potentials on plane transonic flow. Symposium Transsonicum II, Springer Verlag, pp. 306-313, (1976).

[16] Redeker, G.; Schmidt, N.; Müller, R.: Design and experimental verification of a transonic wing for a transport aircraft. AGARD-CP-285 (1980), pp. 13-1 to 13-14.

[17] Redeker, G.; Brandes, H.: Modifikation des transsonischen Profils DFVLR-R4. DFVLR IB 129-81/24 (1981).

[18] Special course on concepts of drag reduction. AGARD-R-654 (1977).

[19] Pfenninger, W.; Reed, H.L.; Degenhardt, J.R.: Design considerations of advanced supercritical low drag suction airfoils. Symp. on Viscous Drag Reduction, Dallas, Tex. (1979), pp. 249-271.

[20] Quast, A.: Laminarprofile für Verkehrsflugzeuge. DFVLR-Mitt. 80-07, (1980).

[21] Althaus, D.; Wortmann, F.X.: Stuttgarter Profilkatalog I. Vieweg Verlag, Braunschweig, 1981.

[22] Eppler, R.: Some new airfoils. NASA-CP-2085, pp. 131-153 (1979).

[23] Horstmann, K.H.; Quast, A.: Widerstandsverminderung durch Blasturbulatoren. DFVLR FB 81-33 (1981).

[24] Quast, A.; Horstmann, K.H.: Anordnung zur Beeinflussung der Strömung an aerodynamischen Profilen. Deutsche Patentanmeldung P3043 567.7.-53.

[25] Horstmann, K.H.; Quast, A.: Tragflügelentwurf für das Weltmeisterschafts-Segelflugzeug SB-11. DFVLR-Nachrichten, Heft 28, pp. 18-20 (1979).

[26] Borchers, U.I.; Mühlbauer, G.: Entwurf, Bau und Erprobung eines verbesserten Propellers für Flugzeuge der Allgemeinen Luftfahrt. Luftfahrtforschung und Luftfahrttechnology, 2. BMFT-Statusseminar, 1980, pp. 257-322.

[27] Köster, H.: Druck- und Widerstandsmessungen am Propellerprofil P2 im Transsonischen Windkanal Braunschweig. DFVLR IB 129-80/20 (1980).

[28] Köster, H.: Messungen am TNT-Propellerprofil im Transsonischen Windkanal Braunschweig. DFVLR IB 129-80/18 (1980).

[29] Max, H.: Aerodynamische Leistungen des Tragflügels neuer Technologie (TNT), ein Vergleich zwischen Auslegungserwartung und Flugversuchsergebnis. Luftfahrtforschung und Luftfahrttechnology, 2. BMFT-Statusseminar (1980).

[30] Zimmer, H.: 7. Zwischenbericht für das ZKP-Vorhaben LKF 7831 "Entwurf, Bau und Erprobung eines Experimentalpropellers in der Leistungsklasse 750 PS. DORNIER Ber. BF 10-2180/82 (1982).

[31] Reichert, G.; Wagner, S.N.: Some aspects of design of rotor airfoil shapes. AGARD-CP-111 (1973), pp. 14-1 to 14-21.

[32] Pearcey, H.H.; Wilby, P.G.; Riley, M.J.; Brotherhood, P.: The derivation and verification of a new rotor profile on the basis of flow phenomena aerofoil research and flight test. AGARD-CP-111 (1973), pp. 15-1 to 15-13.

[33] Thibert, J.J.; Gallot, J.: Advanced research on helicopter blade airfoils. 6th European Rotorcraft and Powered Lift Aircraft Forum, Bristol, 1980.

[34] Körner, H.; Puffert-Meißner, W.: Windkanaluntersuchungen an dünnen superkritischen Profilen. DFVLR FB 82-06 (1982).

[35] Eberle, A.: Entwurf eines dünnen überkritischen Profils MBB A10. MBB-UFE-AERO-MT 268 (1976).

[36] Eberle, A.: Definition eines dünnen überkritischen Profils nach der Whitcomb-Offenlegungsschrift. MBB-UFE-AERO-MT-296 (1977).

[37] Körner, H.; Puffert, W.; Schmidt, W.; Kleiner, H.: Experimentelle Untersuchungen an einem dünnen Profil mit Manöverklappen. DORNIER-DFVLR IB 151-80/14 (1980).